Journal of Power Sources 195 (2010) 2110–2117

Contents lists available at ScienceDirect

Journal of Power Sources

journal homepage: www.elsevier.com/locate/jpowsour

Anodic deposition of manganese oxide electrodes with rod-like structures for application as electrochemical capacitors

Banafsheh Babakhani, Douglas G. Ivey*

Department of Chemical and Materials Engineering, University of Alberta, Edmonton, Alberta, Canada T6G 2V4

ARTICLE INFO

Article history:
Received 12 August 2009
Received in revised form 15 October 2009
Accepted 15 October 2009
Available online 27 October 2009

Keywords:
Electrodeposition
Electrochemical capacitor
Manganese oxide
Electron microscopy
Voltammetry

ABSTRACT

The electrochemical properties of nanocrystalline manganese oxide electrodes with rod-like structures were investigated to determine the effect of morphology, chemistry and crystal structure on the corresponding electrochemical behavior of manganese electrodes. Manganese oxide electrodes of high porosity composed of 1–1.5 μm diameter rods were electrochemically synthesized by anodic deposition from a dilute solution of $Mn(CH_3COO)_2$ (manganese acetate) onto Au coated Si substrates without any surfactants, catalysts or templates under galvanostatic control. The morphology of the electrodes depended on the deposition current density, which greatly influenced the electrochemical performance of the capacitor. Electrochemical property and microstructure analyses of the manganese oxide electrodes were conducted using cyclic voltammetry and microstructural techniques, such as scanning electron microscopy (SEM), transmission electron microscopy (TEM) and X-ray photoelectron spectroscopy (XPS). The synthesized rod-like manganese oxide electrodes at low current densities exhibited a high specific capacitance due to their large surface areas. The largest value obtained was 185 F g^{-1} for deposits produced at .5 mA cm^{-2}. Specific capacity retention for all deposits, after 250 charge–discharge cycles in an aqueous solution of 0.5 M Na_2SO_4, was about 75% of the initial capacity.

1. Introduction

Research on electrochemical capacitors has generated growing interest from both academia and industry in recent years, with efforts focused on developing safe, stable, high energy/power density and low cost materials. Electrochemical capacitors are considered as a promising power storage device for back up power storage, peak power sources and hybrid electric and fuel cell vehicles, due to their high specific capacitance, high charge/discharge rate, long cycle life and excellent reversibility [1–4].

Based on the intrinsic principles of charge storage and discharge in electrochemical capacitors, the energy stored is either capacitive (non-faradaic) or pseudocapacitive (faradaic) in nature. The non-faradaic process relies on charge separation at the interface between the electrode and the ionic solution giving rise to an electrical double layer, whereas the faradaic process consists of redox reactions occurring within the active electrode materials [2]. Based on the type of supercapacitance to be utilized, electrochemical capacitors can be made from various materials including carbon [5], conducting polymers [6–10], noble metal oxides such as RuO_2 [11–13] and IrO_2 [14] and transition metal oxides such as MnO_2 [15], NiO [16], Co_2O_3 [17], FeO [18], TiO_2 [19], SnO_2 [20], V_2O_5 [21–23] and MoO [24]. Among the transition metal oxides, manganese-based oxides have been widely studied for electrochemical capacitors and batteries, because of their high energy density, low cost, natural abundance and environmentally friendly nature. A Mn^{4+}/Mn^{3+} redox system involving single-electron transfer is responsible for MnO_2 pseudocapacitive behavior. Manganese oxide stores electrochemical energy by simultaneous injection of electrons and charge-compensating cations, as with other electroactive transition metal oxides, which makes it potentially useful for charge storage applications. Amorphous/crystalline manganese oxide shows high specific capacitance due to the utilization of both electric double layer and redox effects. Hydrated manganese oxides may exhibit specific capacitances within the 100–200 F g^{-1} range in alkali salt solutions depending on the processing conditions. Although these values are much lower than those for RuO_2 (600–1000 F g^{-1}), manganese oxide is still considered as an appropriate replacement for noble metal oxides in electrochemical capacitors [25–30]. In order to synthesize manganese oxide electrodes, several chemical techniques such as sol–gel [31] deposition from colloidal suspensions [32] and electrochemical deposition [25–30] have been adopted. Electrochemical deposition has some advantages over other techniques, e.g., the mass and thickness of

* Corresponding author at: Department of Chemical and Materials Engineering, University of Alberta, 7th Floor ECERF Building, Edmonton, Alberta, Canada T6G 2V4. Tel.: +1 780 492 2957; fax: +1 780 492 2881.
E-mail address: doug.ivey@ualberta.ca (D.G. Ivey).

0378-7753/$ – see front matter © 2009 Elsevier B.V. All rights reserved.
doi:10.1016/j.jpowsour.2009.10.045

the metal oxide film is easily controllable simply by adjusting the current, temperature and electrolyte chemical composition [33].

Past research has indicated that the electrochemical characteristics of electrode materials, such as specific capacitance and voltammetric capacitance reduction with cycling, are greatly dependent on the grain size, surface area, morphology, chemistry and crystal structure [34,35]. It has been noted that partial dissolution of MnO_2 films into the electrolyte during cycling, leading to gradual loss of active electrode materials, is a major reason for capacitance reduction with an increasing number of charge/discharge cycles, and is attributed to the disproportionation of trivalent manganese [35,36]. Gradual mechanical failure of the electrode materials can also lead to capacitance fading [37]. In addition, oxygen evolution strongly influences the cycle life of manganese dioxide by affecting the electrode/current collector interface and increasing the equivalent series resistance of the cell [10].

It has been shown that a combination of manganese oxide with other materials, such as conducting polymers, may reduce both MnO_2 dissolution and mechanical failure and provide excellent electrochemical and mechanical properties for electrochemical energy storage [38,39]. In addition, electrode materials with ordered, high surface area structures can enhance the electrochemical characteristics and maintain them after repeated cycling [10,35]. One-dimensional (1D) nanostructured materials provide short transport/diffusion path lengths for both ions and electrons, leading to faster kinetics and also large specific surface areas, resulting in high charge/discharge capacities [38,40]. Templates or catalysts have been widely used to grow 1D nanostructured materials. Templates are used to confine the growth of wires, while catalysts may act as the energetically favorable sites for the adsorption of reactant molecules. An anodic aluminum oxide (AAO) template offers a promising route to synthesize high surface area, ordered manganese oxide nanowire array electrodes. This method is not, however, easy to use in practical applications due to the fragility of the AAO template. Moreover, dissolution of the template is complicated and the morphology of the materials is often poor, because the AAO membrane pores can become impregnated with the reagents producing smooth-faced materials [41–43].

It is possible to prepare 1D nanostructured manganese oxides with desirable morphologies (e.g., rod-like structures) under controlled conditions without the presence of catalysts or templates. The formation of 1D manganese oxide structures may be kinetically preferable for many substances under certain conditions. In the present study, 1D manganese oxide electrodes are synthesized through the oxidation of Mn^{2+} without catalysts or templates in order to determine the relationship between the physicochemical features of manganese oxide electrodes and corresponding electrochemical behavior. It is expected that this work may provide new technical insights to improve the electrochemical properties and cyclability of manganese oxide electrodes for applications to electrochemical capacitors.

2. Experimental procedure

Manganese oxide coatings were anodically electrodeposited from two different types of dilute solutions (0.01 M $MnSO_4$ and 0.01 M $Mn(CH_3COO)_2$) onto Au (500 nm thick) coated Si substrates with dimensions of 15 mm × 8 mm × 1 mm using a hot water bath under galvanostatic control, i.e., 5–30 mA cm^{-2}. A platinum counter electrode was placed vertically 20 mm away from a vertical Au coated Si working electrode. The electrolyte pH value and electrolyte temperature were adjusted to 6.5 and 60 °C, respectively. Deposition times were 10 min for both solutions and all current densities. Before anodic electrodeposition, the Au coated Si substrates were cleaned with acetone and then ethanol. During electrodeposition, agitation was applied with a magnetically driven Teflon® coated stirring bar at a speed of 300 rpm. After electrodeposition the working electrodes were rinsed with deionized water, dried at 100 °C for 60 min in air to remove any residual water and then stored in a vacuum desiccator before further analysis. The mass of the manganese oxide deposits on the Au coated Si electrodes was determined from the weight difference between the Au coated Si electrode before and after anodic deposition, as measured using a microbalance (Sartorius BP211D) with an accuracy of 10 μg. The specific deposit mass was controlled to be 0.15–0.20 mg cm^{-2}.

2.1. Materials characterization

The morphology and chemistry of the manganese oxide deposits, in as-deposited and cycled electrodes, were investigated using a Hitachi S-2700 scanning electron microscope (SEM) operated at 20 kV and equipped with an ultra-thin window (UTW) X-ray detector. Chemical state analysis was performed by X-ray photoelectron spectroscopy (XPS) using a Kratos AXIS Ultra X-ray photoelectron spectrometer with a monochromatic Al source (210 W with a pass energy of 20 eV and a step size of 0.1 eV). Curve fitting and background subtraction were performed using Casa XPS software. The crystal structure of the manganese oxide rods was investigated using selected area electron diffraction (SAED) of samples prepared for transmission electron microscopy (TEM). A JEOL 2010 transmission electron microscope (TEM), operated at 200 kV, and equipped with a Noran ultra-thin window (UTW) X-ray detector was used. An electron transparent sample was prepared by scraping some of a deposit from the substrate and then ultrasonically dispersing the residue in methanol for 10 min. One or two drops of the suspension were deposited onto a C-coated, Cu grid (300 mesh). After evaporation of the methanol, samples were ready for TEM analysis.

2.2. Electrochemical behavior

In order to determine the electrochemical behavior of the manganese oxide electrodes, a Gamry PC4/750 potentiostat/galvanostat was used for cyclic voltammetry (CV) in an electrolyte containing 0.5 M Na_2SO_4 at room temperature. A three-electrode cell configuration was applied: a working electrode (manganese oxide deposit on a Au coated Si), a platinum (Pt) mesh as a counter electrode and a saturated calomel electrode (SCE) as the reference electrode. Cyclic voltammograms were recorded between −0.1 and 0.8 V vs. SCE at a scanning rate of 20 mV s^{-1}. For consistency, all CV scans were done using fresh deposits.

3. Results and discussion

3.1. Morphology and crystal structure of as-prepared manganese oxide electrodes

The chemistry, morphology and crystal structure of manganese oxide coatings can be manipulated by adjusting the deposition parameters, such as complexing agents, deposition current density, voltage and pH. The morphology and crystal structure of the as-prepared manganese oxide coatings obtained from solutions composed of 0.01 M $MnSO_4$ or 0.01 M $Mn(CH_3COO)_2$ (acetate acts as complexing agent) were analyzed using SEM and TEM. Plan view secondary electron (SE) images, shown in Fig. 1a and c, reveal two different types of morphology for the resultant oxides. The SE micrograph of the oxide deposited from a solution containing

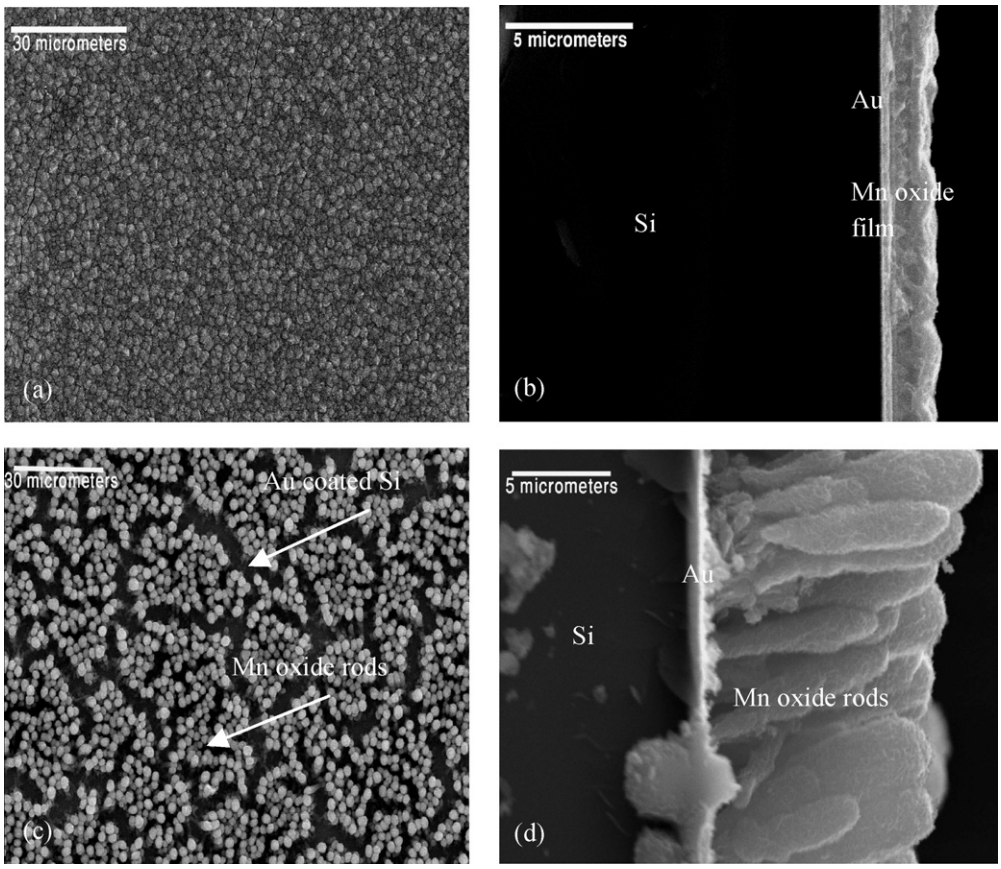

Fig. 1. SE plan view and cross-section images of manganese oxide prepared from a solution of (a) and (b) 0.01 M $MnSO_4$ at $i = 30\ mA\ cm^{-2}$; (c) and (d) 0.01 M $Mn(CH_3COO)_2$ at $i = 5\ mA\ cm^{-2}$ (pH = 6.5).

0.01 M $MnSO_4$ (Fig. 1a and b) is continuous but relatively porous, which is typical for electrochemically active MnO_2 [24]. In contrast, for deposits prepared from the 0.01 M $Mn(CH_3COO)_2$ solution, free-standing rods (about 10 μm long and less than 1.5 μm in diameter) are clearly visible (Fig. 1c and d). In this case, manganese oxide may preferably grow on energetically favorable sites under galvanostatic control resulting in the highly porous structure. The rod-like structures exhibit large specific surface areas, which promote efficient contact between the active material and the electrolyte, providing more active sites for electrochemical reactions. It should be noted that structures with porosity and interconnectivity supply additional accessible space for ions while maintaining sufficient conductivity for solid-state electronic transfer. Significantly enhanced capacitance and high cycling rate capability can, therefore, be expected. Smaller diameter rods will provide larger specific surface areas for electrolyte access to improve the electrochemical capacity. Moreover, rod-like structures can provide short diffusion path lengths to both ions and electrons and also sufficient porosity for electrolyte penetration giving rise to high charge/discharge rates [38,40].

Since deposits produced from the $Mn(CH_3COO)_2$ solutions exhibited a more promising morphology, the rest of paper focuses on manganese oxide deposits obtained from the Mn acetate solutions.

The morphology of the manganese oxide rods, prepared from the manganese acetate solutions, can be controlled by varying the deposition current density. This is shown in Fig. 2, where the synthesized manganese oxide at lower deposition current densities (Fig. 2a–e) has more uniform, vertical and free-standing rods. At higher deposition current densities (Fig. 2c and f), the synthesized manganese oxide tends to form interconnected rods. As shown later in this paper, the uniform microstructure provides better electrochemical behavior.

Individual manganese oxide rods were examined in more detail by TEM. A bright field (BF) image of two rods, from a sample deposited at 5 mA cm^{-2}, is shown in Fig. 3a, where a fibrous surface is visible. An SAED pattern and a dark field (DF) image of the circled region shown in Fig. 3a are shown in Fig. 3b. The DF image was obtained using part of the first two diffraction rings. The diffraction pattern reveals that the rods are polycrystalline and the DF image shows that the oxide grains are less than 10 nm in diameter. The small crystallite size and fibrous nature of the surface should enhance diffusion transport of both electrons and ions, resulting in faster kinetics. The SAED pattern was indexed to a NaCl-type crystal structure (FCC with space group corresponding to $Fm\bar{3}m$) with a lattice parameter of 0.445 nm. MnO has a NaCl-type structure with a lattice parameter of 0.4534 nm, which is close to the value for the experimental pattern.

3.2. XPS analysis

XPS was applied to determine the oxygen anion content and the oxidation state of the Mn cations in manganese oxide deposits obtained from 0.01 M $Mn(CH_3COO)_2$ solutions. All XPS spectra for the deposits were essentially the same; representative Mn 2p and O 1s spectra are shown in Fig. 4a and b. The Mn 3s spectrum can be used to approximate the valence of Mn cations using the 3s splitting widths. There is an approximately linear relationship between the Mn oxidation state and the 3s splitting width (ΔE) [24]. Unfortunately, the Au seed layer produced Au 4f peaks which overlapped with the Mn 3s peaks making it impossible to determine the 3s splitting widths. The Mn 2p spectrum was examined instead

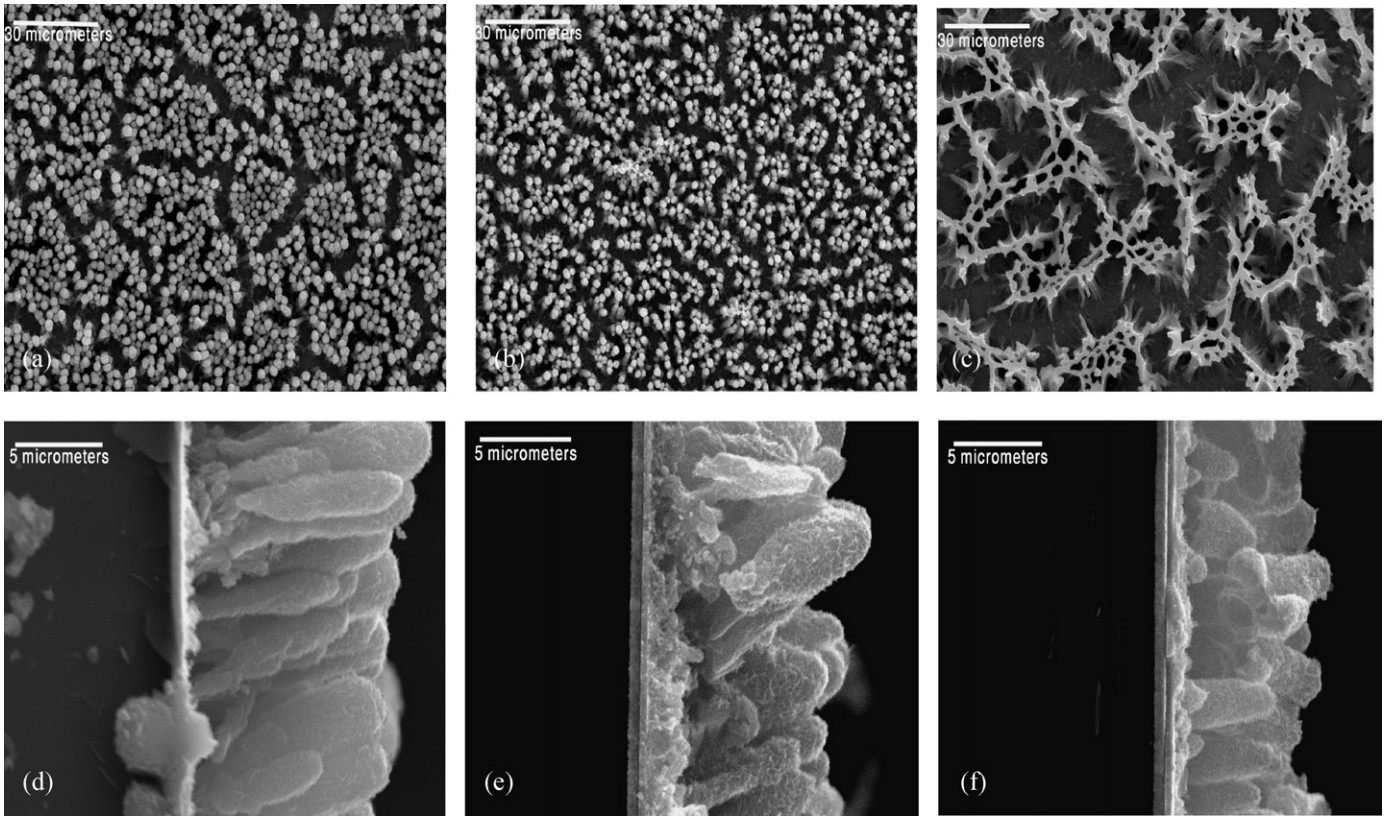

Fig. 2. SE plan view and cross-section images of Mn oxide deposits prepared from a 0.01 M $Mn(CH_3COO)_2$ solution at (a) and (d) $i = 5\ mA\ cm^{-2}$; (b) and (e) $i = 15\ mA\ cm^{-2}$; (c) and (f) $i = 30\ mA\ cm^{-2}$ (pH = 6.5).

(Fig. 4a). The $2p_{3/2}$ binding energy peak is located at 642.25 eV and the $2p_{1/2}$ peak is located at 653.72 eV. The peak positions and the separation between Mn $2p_{3/2}$ and $2p_{1/2}$, which is about 11.47 eV, can be attributed to a Mn valence of 4+ and/or 3+.

The O 1s spectrum was considered as well. The O 1s spectrum can be deconvoluted into three major bond components: oxide (O^{2-}), hydroxide (OH^-) and residual structural water (Fig. 4b). This provides useful information about the state of oxygen bonding, hydration of the oxide nanocrystals and the valence of manganese cations. The formation of a hydrated film is considered to be critical to the capacitance mechanism as the fraction of reaction sites accessible to the faradaic process is larger when the deposit is in a hydrous form [44]. Based on the O 1s XPS spectrum, the deposit consists of MnO_2 (Mn4+) and MnOOH (Mn3+) (which is thermodynamically favorable relative to $Mn(OH)_2$). For the deposit in Fig. 4b, the amounts of MnO_2 and MnOOH were determined to be 58% and 37%, respectively. Other deposits had similar distributions.

The XPS results appear to contradict the TEM diffraction analysis, where a NaCl-type structure was identified and MnO has a NaCl-type structure. However, previous work by one of the authors showed that MnO_2 prepared from an ethylenediaminetetraacetic acid (EDTA)-containing solution had a NaCl-type structure [45]. The structure was metastable and was described as an FCC array of oxygen anions with Mn cations randomly occupying the octahe-

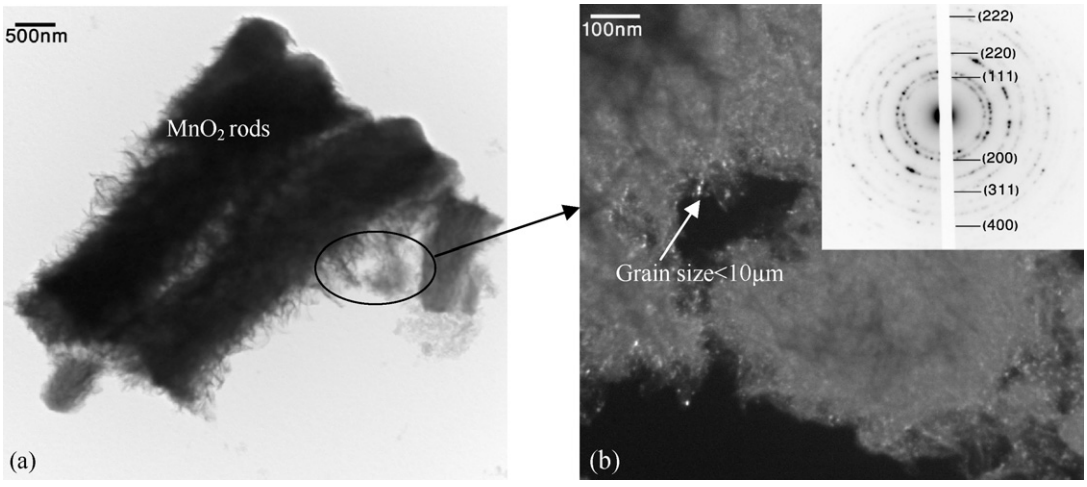

Fig. 3. Morphology and crystal structure of manganese oxide prepared from a 0.01 M $Mn(CH_3COO)_2$ solution at $i = 5\ mA\ cm^{-2}$. (a) TEM BF image and (b) TEM DF image and SAED pattern.

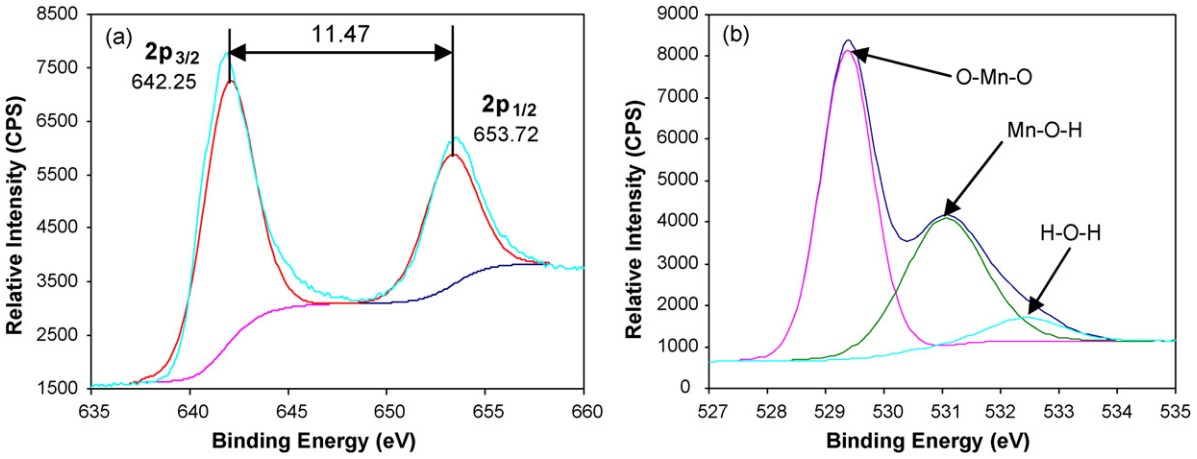

Fig. 4. Typical (a) XPS Mn 2p spectrum and (b) XPS O 1s spectrum for manganese oxide deposited from a 0.01 M $Mn(CH_3COO)_2$ solution. This particularly oxide was deposited at $i = 5\,mA\,cm^{-2}$.

dral interstices. The MnO_2 formula was accounted for by cation vacancies on many of the octahedral interstices in the FCC unit cell [46]. Therefore, the nanocrystalline phase in the deposit can be considered to be MnO_2. No other crystalline phases were detected through TEM electron diffraction, which suggests that MnOOH may be amorphous.

3.3. Electrochemical behavior of Mn oxide electrodes

The electrochemical properties of the oxide coatings were evaluated using CV curves which were scanned at a rate of $20\,mV\,s^{-1}$ for up to 250 cycles in a 0.5 M Na_2SO_4 solution. A representative plot for a deposit obtained at $5\,mA\,cm^{-2}$ from the $Mn(CH_3COO)_2$ solution is shown in Fig. 5. A relatively low scan rate was used to ensure redox transformation for a relatively large fraction of the electrode material. The cyclic voltammogram initially exhibits a rectangular-shaped profile, which is characteristic of ideal capacitive behavior. As the cycling number increases, the area under the voltammetric curves decreases, which is typical for electrochemically active MnO_2. Also, the voltammetric curves exhibit broad anodic and cathodic peaks centered at about 0.55 and 0.42 V. These are attributed to cation deintercalation upon oxidation and cation intercalation upon reduction. It has been noted that both diffusion and redox reactions contribute to charge transfer for electrochemical charge storage in MnO_2 materials. However, the partial cation intercalation/deintercalation reactions contribute more to the total capacitance with increased cycling, which intensifies the anodic and cathodic peaks [46]. Also, morphology changes during cycling may facilitate electrolyte transport and reduce solid-state diffusion distances for ions into the oxides, which would increase the prominence of cation intercalation/deintercalation reactions [47].

The specific capacitance C ($F\,g^{-1}$) of the active material was determined by integrating either the oxidative or the reductive parts of the cyclic voltammogram curve to obtain the voltammetric charge Q (C). This charge was subsequently divided by the mass of active material m (g) in the electrode and the width

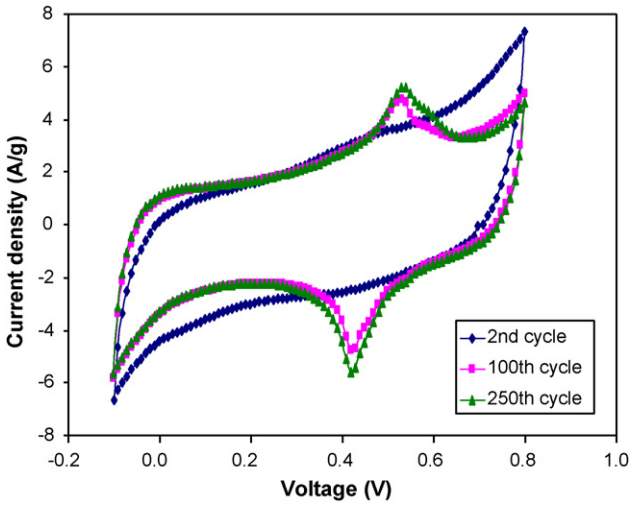

Fig. 5. Representative cyclic voltammograms taken from manganese oxide electrodes prepared from 0.01 M $Mn(CH_3COO)_2$ at $i = 5\,mA\,cm^{-2}$ (cycled at $20\,mV\,s^{-1}$ for up to 250 cycles).

of the potential window of the cyclic voltammogram ΔE (V), i.e., $C = Q/(\Delta E m)$. The original specific capacitances are taken after the second cycle, because after the first charge/discharge cycle both electrodes demonstrate a small irreversible capacity in each sequential cycle. According to the charge/discharge behavior of transition metal oxides, the second CV curve differs considerably from the first because there have been drastic structural or textural modifications. The large irreversible capacity occurring only in the first cycle may be caused by decomposition reactions in the electrolyte and the formation of a solid electrolyte interphase film on the surface of the manganese oxide electrode.

Manganese oxide rods synthesized at lower deposition current densities had better specific capacitances. The specific capacitance

Table 1
Specific capacitance values for manganese oxide deposits from $Mn(CH_3COO)_2$ solutions at different current densities.

Deposition current density ($mA\,cm^{-2}$)	Specific capacitance after second cycle ($F\,g^{-1}$)	Specific capacitance after 100 cycles ($F\,g^{-1}$)	Specific capacitance after 250 cycles ($F\,g^{-1}$)	Specific capacitance decrease after 250 cycles (%)
5	185	175	139	25
10	163	154	128	22
15	155	145	117	24
20	138	130	108	22
30	120	108	94	23

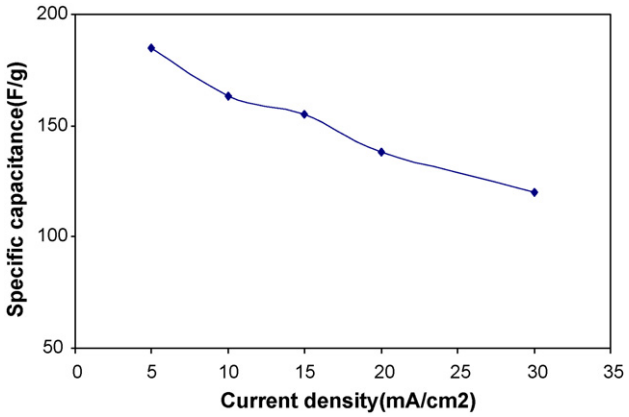

Fig. 6. Specific capacitance of manganese oxide nanocrystals with a rod-like structure prepared from a 0.01 M $Mn(CH_3COO)_2$ solution at different current densities and cycled at 20 mV s^{-1} (second cycle).

values for MnO_2 with rod-like structures ($Mn(CH_3COO)_2$ solution), synthesized at different deposition current densities, are shown in Fig. 6. The deposit prepared at a current density of 5 mA cm^{-2} had the highest specific capacitance. Capacitance decreased almost linearly with increasing deposition current density. The specific capacitance values for manganese oxide deposits obtained at different current densities after 2, 100 and 250 cycles in 0.5 M Na_2SO_4 are listed in Table 1. After 250 cycles at 20 mV s^{-1}, the specific capacitance retention is about 75% of the original value for all deposits.

3.4. Morphology and crystal structure of cycled manganese oxide

Cycled samples were examined in the SEM to monitor any morphological changes. Fig. 7a–c shows images of manganese oxide electrodes synthesized by anodic deposition from 0.01 M $Mn(CH_3COO)_2$ solutions at different deposition current densities after cycling at 20 mV s^{-1} for 250 cycles. There is not much change in the morphology of the deposits prepared at lower deposition current densities (relative to the as-deposited morphology, Fig. 2). However, the rod-like structure from samples prepared at high current densities has evolved into a petal-like morphology after cycling. This may be attributed to partial dissolution of manganese oxide during cycling, since the charge/discharge process in MnO_2 involves a redox reaction between the III and IV oxidation states of Mn. Some of the MnO_2 inevitably dissolves into the 0.5 M Na_2SO_4 electrolyte and then redeposits.

A TEM BF image and corresponding SAED pattern for a manganese oxide deposit, prepared from the 0.01 M $Mn(CH_3COO)_2$ solution at i = 5 mA cm^{-2} after 250 cycles at 20 mV s^{-1}, are shown in Fig. 8. One of the rods from the deposit is clearly visible in Fig. 8a, with an internal fibrous structure. Careful examination of the SAED pattern (Fig. 8b) reveals a total of five main diffraction rings with d-spacings of ~0.436, 0.242, 0.211, 0.168 and 0.142 nm. The d-spacings and intensities of these diffracted rings, with the exception of the 1st ring at 0.436 nm, are consistent with that of MnO_2 with an ε-NiAs-type crystal structure (HCP with space group corresponding to $P6_3/mmm$) with lattice parameters of a = 0.280 nm and c = 0.445 nm. In this structure, Mn4+ cations randomly occupy 50% of the octahedral positions of the hexagonal close packed

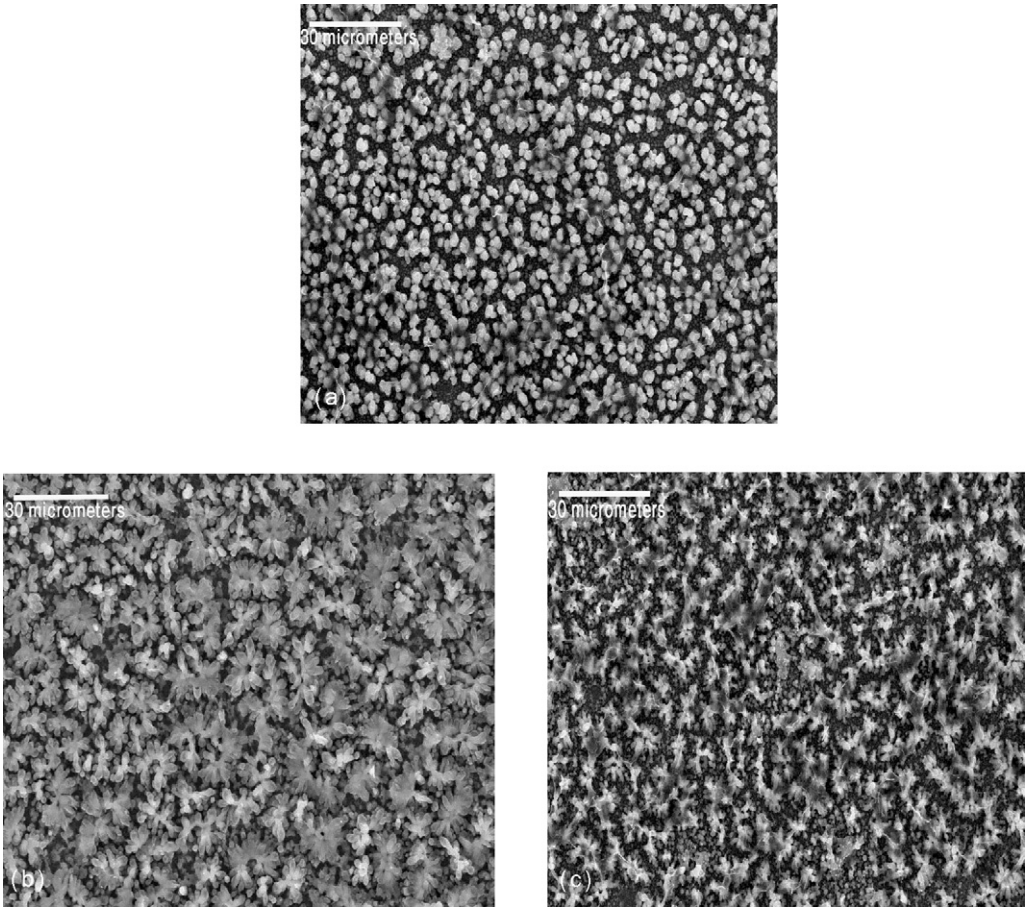

Fig. 7. SE images of manganese oxide prepared from a solution of 0.01 M $Mn(CH_3COO)_2$ at (a) i = 5 mA cm^{-2}; (b) i = 15 mA cm^{-2}; (c) at i = 30 mA cm^{-2} solution after 250 cycles at 20 mV s^{-1} (pH = 6.5).

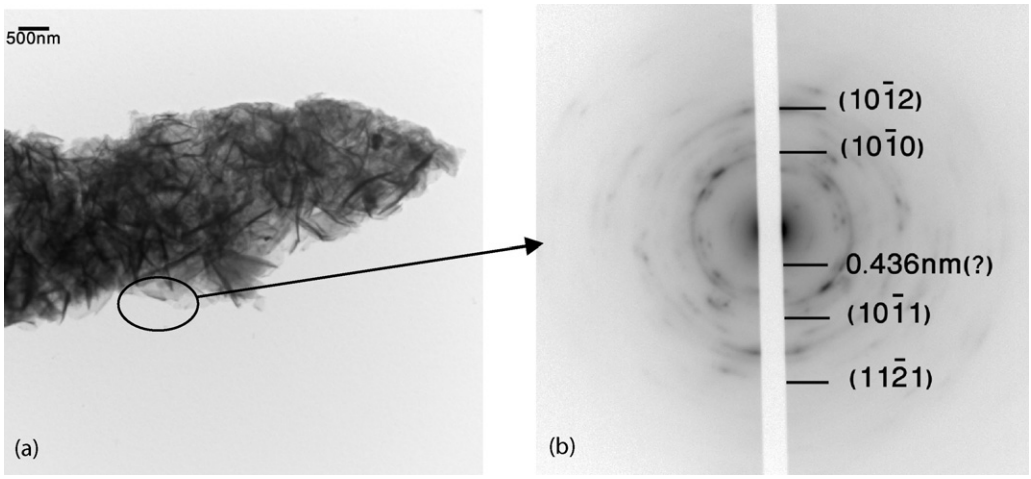

Fig. 8. Morphology and crystal structure of manganese oxide prepared from a 0.01 M $Mn(CH_3COO)_2$ solution at $i = 5\,mA\,cm^{-2}$ after 250 cycles at $20\,mV\,s^{-1}$. (a) TEM BF image and (b) SAED pattern.

(hcp) oxygen sublattice [48]. The four diffracted rings (2nd–5th) are indexed as the (1 0 $\bar{1}$ 0), (1 0 $\bar{1}$ 1), (1 0 $\bar{1}$ 2) and (11$\bar{2}$1) reflections based on the ε-MnO_2 structure as shown in Fig. 8. The 1st ring can be indexed to (0 0 0 1), although the (0 0 0 1) reflection is generally not allowed for the NiAs-type structure. However, given the highly defective nature of the deposit, the (0 0 0 1) reflection may become allowable. The crystal structure of manganese oxide has changed to a more close packed structure after 250 cycles in the 0.5 M Na_2SO_4 solution. Therefore, fewer electrochemically active sites are available for fast ionic transport and charge transfer, which may account for at least some of the capacitance fading with increasing cycle number.

Several factors can contribute to capacitance fading, including the change in crystal structure discussed in the previous paragraph. The decrease in capacity after cycling can also be attributed to increased electrode resistance with increasing cycle number. A possible reason is that during the charge/discharge processes, catalytic manganese metal may be isolated by nonconducting materials, such as Na_2O or a passive film, which form as a side-reaction byproduct between water and sodium [49]. The evolution from equiaxed rods to a petal-shape, which reduces the effective surface area of the manganese oxide electrodes, may also contribute to capacitance fading with increasing cycle number [45]; however, this effect may be minor for the electrodes in this work. All electrodes showed similar amounts of fading (23–25%) whether or not a petal-shape morphology formed on cycling.

It has been shown previously that the physicochemical feature evolution in manganese oxide electrodes has significant effects on the electrochemical behavior [45]. Manganese oxide rods synthesized at lower deposition current densities provide good capacitance behavior and reasonable capacitance retention after cycling. The Mn oxide coatings synthesized at a deposition current density of $5\,mA\,cm^{-2}$ show the highest specific capacitance ($185\,F\,g^{-1}$) and maintain 75% of their capacitance after cycling.

All manganese oxide electrodes prepared from $Mn(CH_3COO)_2$ solutions have a nanocrystalline structure. It should be noted that the nanocrystalline structure of the hydrated manganese oxide rods helps to decrease capacity fading. As previously mentioned, redox reactions (intercalation of Na^+ ions in the electrode during reduction and deintercalation on oxidation) contribute to charge transfer for electrochemical charge storage in MnO_2 materials. In well crystallized electrode materials, Na^+ ion intercalation is often accompanied with lattice structure distortion, leading to significant capacity fading with successive charge/discharge cycles [50]. In contrast, a nanocrystalline structure is less well packed with a higher tendency for structural accommodation as well as more open free space during Na^+ ion intercalation and diffusion.

4. Conclusions

Nanocrystalline manganese oxide coatings were anodically electrodeposited from 0.01 M $Mn(CH_3COO)_2$ solutions onto the Au coated Si substrates under galvanostatic control. The morphology of the manganese oxide deposits with rod-like structures depends on the current density. As such, deposits synthesized at a current density of $5\,mA\,cm^{-2}$ showed the highest specific capacitance ($185\,F\,g^{-1}$). As-deposited manganese oxide, prepared at different current densities, was made up of MnO_2 with a NaCl-type crystal structure and MnOOH which was likely amorphous.

The loss in capacticance with electrochemical cycling, which was 23–25% for all manganese oxide deposits, can be attributed to several factors. Increased manganese oxide electrode resistance with increasing cycle number can decrease capacitance. In addition, deposits synthesized at higher current densities underwent a microstructural change on cycling to a petal-shape morphology; this structure reduced the specific surface area of the manganese oxide leading to the capacitance fading. Finally, MnO_2 transformed to a more ordered hexagonal NiAs-type crystal structure after cycling. As such, fewer electrochemically active sites were available for fast ionic transport and charge transfer resulting.

Acknowledgements

The financial support from the Natural Sciences and Engineering Research Council (NSERC) of Canada is gratefully acknowledged. The authors would like to thank the Alberta Centre for Surface Engineering and Science (ACSES) for providing the XPS analysis. R. Eslahpazir is also acknowledged for assisting with the TEM analysis.

References

[1] S. Sarangapani, B.V. Tilak, C.P. Chen, J. Electrochem. Soc. 143 (1996) 3791.
[2] B.E. Conway, Electrochemical Supercapacitors, Kluwer Academic/Plenum Press, New York, 1999.
[3] R.N. Reddy, R.G. Reddy, J. Power Sources 132 (2004) 315.
[4] A. Burke, J. Power Sources 91 (2000) 37.
[5] H.A. Andreas, B.E. Conway, Electrochim. Acta 51 (2006) 6510.
[6] C. Peng, S.W. Zhang, D. Jewell, Prog. Nat. Sci. 18 (2008) 777.
[7] S. Cho, S.B. Lee, Acc. Chem. Res. 41 (2008) 699.
[8] C. Peng, J. Jin, G. Chen, Electrochim. Acta 53 (2007) 525.
[9] A. Malinauskas, J. Malinauskiene, A. Ramanavicius, Nanotechnology 16 (2005) 51.

[10] D. Belanger, T. Brousse, J.W. Long, Electrochem. Soc. Interf. 17 (1) (2008) 49.
[11] W. Sugimoto, K. Yokoshima, Y. Murakami, Electrochim. Acta (2006) 1742.
[12] V.D. Patake, C.D. Lokhande, O.S. Joo, Appl. Surf. Sci. 255 (2009) 4192.
[13] Y.R. Ahn, M.Y. Song, S.M. Jo, C.R. Park, Nanotechnology 17 (2006) 2865.
[14] C.C. Hu, Y.H. Huang, K.H. Chang, J. Power Sources 108 (2002) 117.
[15] J. Jiang, A. Kucernak, Electrochim. Acta 27 (2002) 2381.
[16] P.A. Nelson, J.R. Owen, J. Electrochem. Soc. 150 (2003) 1313.
[17] S.G. Kandalkar, J.L. Gunjakar, C.D. Lokhande, Appl. Surf. Sci. 254 (2008) 5540.
[18] L. Cheng, H. Li, Y. Xia, J. Solid State Electrochem. 10 (2006) 405.
[19] M. Hibino, K. Abe, M. Mochizuki, M. Miyayama, J. Power Sources 126 (2004) 139.
[20] N. Miura, S. Oonishi, K. Rajendra, Electrochem. Solid State Lett. 7 (2004) 247.
[21] D.L. Silva, R.G. Delattore, G. Pattanaik, J. Electrochem. Soc. 155 (2008) 14.
[22] C.C. Hu, C.M. Huang, K.H. Chang, J. Power Sources 185 (2008) 1594.
[23] X. Zhou, H. Chen, D. Shu, C. He, J. Phys. Chem. Sol. 70 (2009) 495.
[24] M. Nakayama, A. Tanaka, Y. Sato, Langmuir 21 (2005) 5907.
[25] S.E. Chun, S.I. Pyun, G.J. Lee, Electrochim. Acta 51 (2006) 6479.
[26] C.C. Hu, C.C. Wang, J. Electrochem. Soc. 150 (2003) A1079.
[27] M.S. Wu, P.J. Chiang, Electrochem. Commun. 8 (2006) 383.
[28] M. Nakayama, T. Kanaya, R. Inoue, Electrochem. Commun. 9 (2007) 1154.
[29] X. Wang, Y. Li, J. Chem. Eur. 9 (2003) 300.
[30] M. Toupin, T. Brousse, D. Belanger, Chem. Mater. 16 (2004) 3184.
[31] S.C. Pang, M.A. Anderson, J. Mater. Res. 15 (2000) 2096.
[32] S.F. Chin, S.C. Pang, M.A. Anderson, J. Electrochem. Soc. 149 (2000) A379.
[33] G.H.A. Therese, P.V. Kamath, Chem. Mater. 12 (2000) 1195.
[34] T. Brousse, M. Toupin, R. Dugas, L. Athouel, J. Electrochem. Soc. 153 (2006) 2171.
[35] K. Naoi, P. Simon, Electrochem. Soc. Interf. 17 (1) (2008) 34.
[36] S. Comaba, A. Ogata, T. Tsuchikawa, Electrochem. Commun. 10 (2008) 1435.
[37] Y.C. Hsieh, K.T. Lee, Y.P. Lin, N.L. Wu, S.W. Donne, J. Power Sources 177 (2008) 660.
[38] R. Liu, S.B. Lee, J. Am. Chem. Soc. 130 (2008) 2942.
[39] R.K. Sharma, A.C. Rastogi, S.B. Desu, Electrochim. Acta 53 (2008) 7690.
[40] C.C. Hu, K.H. Chang, M.C. Lin, Y.T. Wu, Nano Lett. 6 (2006) 2690.
[41] F. Cheng, Z. Thao, J. Liang, J. Chen, Chem. Mater. 2 (2008) 667.
[42] G.Y. Zhao, C.L. Xu, H.L. Li, J. Power Sources 163 (2007) 1132.
[43] Y. Xia, P. Yang, Y. Sun, Y. Wu, Adv. Mater. 15 (2000) 353.
[44] B. Djurfors, J.N. Broughton, M.J. Brett, D.G. Ivey, Acta Mater. 53 (2005) 957.
[45] W. Wei, X. Cui, W. Chen, D.G. Ivey, J. Power Sources 186 (2009) 543.
[46] W. Wei, W. Chen, D.G. Ivey, J. Phys. Chem. 111 (2007) 10398.
[47] W. Wei, X. Cui, W. Chen, D.G. Ivey, Electrochim. Acta 54 (2009) 2271.
[48] C.H. Kim, Z. Akase, L. Zhang, A.H. Heuer, J. Solid State Chem. 179 (2006) 753.
[49] M.S. Wu, P.C.J. Chiang, J.T. Lee, J.C. Lin, J. Phys. Chem. B 109 (2005) 23279.
[50] D. Liu, Q. Zhang, P. Xiao, B.B. Garcia, Chem. Mater. 20 (2008) 1376.